Bioresource Technology 365 (2022) 128071

Contents lists available at ScienceDirect

Bioresource Technology

journal homepage: www.elsevier.com/locate/biortech

Improving green hydrogen production from *Chlorella vulgaris* via formic acid-mediated hydrothermal carbonisation and neural network modelling

Zita Gruber [a], Andras Jozsef Toth [a], Alfréd Menyhárd [b], Peter Mizsey [c], Mikołaj Owsianiak [d], Daniel Fozer [d,*]

[a] Faculty of Chemical Technology and Biotechnology, Budapest University of Technology and Economics, Műegyetem rkp. 3., Budapest, Hungary
[b] Department of Physical Chemistry and Materials Science, Laboratory of Plastics and Rubber Technology, Budapest University of Technology and Economics, H-1111 Budapest, Műegyetem rkp. 3. H. ép. I, Hungary
[c] Department of Fine Chemicals and Environmental Technology, University of Miskolc, Egyetem út, 3515 Miskolc, Hungary
[d] Department of Environmental and Resource Engineering, Quantitative Sustainability Assessment, Technical University of Denmark, Produktionstorvet, Building 424, DK-2800 Kgs. Lyngby, Denmark

HIGHLIGHTS

- Formic acid mediator in hydrothermal carbonisation raises biomass-to-H_2 conversion.
- Artificial neural network accurately predicts HTC yields and products properties.
- The HTC gas yield is increased from 1.67 to 13.42 mol kg^{-1} using an acid mediator.
- Higher combined severity factor (>1.5) intensifies green hydrogen evolution.
- For dilute suspensions, CSF>2.8 is needed to maintain a high H_2 yield (3 mol kg^{-1}).

GRAPHICAL ABSTRACT

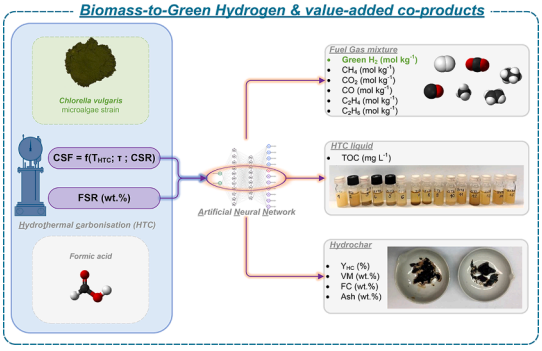

ARTICLE INFO

Keywords:
Hydrothermal carbonisation
Microalgae
Gas formation
Green hydrogen
Machine learning
Combined severity factor

ABSTRACT

This study investigates the formic acid-mediated hydrothermal carbonisation (HTC) of microalgae biomass to enhance green hydrogen production. The effects of combined severity factor (CSF) and feedstock-to-suspension ratio (FSR) are examined on HTC gas formation, hydrochar yield and quality, and composition of the liquid phase. The hydrothermal conversion of *Chlorella vulgaris* was investigated in a CSF and FSR range of −2.529 and 2.943; and 5.0 wt.% – 25.0 wt.%. Artificial neural networks (ANNs) were developed based on experimental data to model and analyse the HTC process. The results show that green hydrogen formation can be increased up to 3.04 mol kg^{-1} by applying CSF 2.433 and 12.5 wt.% FSR reaction conditions. The developed ANN model (BR-2-11-9-11) describes the hydrothermal process with high testing and training performance (MSE_z = 1.71E−06 & 1.40E−06) and accuracy (R^2 = 0.9974 & R^2 = 0.9781). The enhanced H_2 yield indicates an effective alternative green hydrogen production scenario at low temperatures using high-moisture-containing biomass feedstocks.

* Corresponding author.
E-mail address: danfo@dtu.dk (D. Fozer).

https://doi.org/10.1016/j.biortech.2022.128071
Received 28 August 2022; Received in revised form 29 September 2022; Accepted 1 October 2022
Available online 17 October 2022

1. Introduction

The transition of modern societies towards net zero emissions requires the extensive use of hydrogen in industrial processes (Henry et al., 2020). The global hydrogen requirement is expected to exceed 200 Mt by 2030, but only 38% of the demand is projected to be synthesised via water electrolysis (IEA, 2021). The urgent need for high-volume hydrogen production call attention to alternative green (i.e., biomass-derived) technological solutions that could mitigate the use of fossil fuels for synthesising H_2.

Among thermochemical hydrogen producing processes, gasification and pyrolysis are established technologies, but undesired co-products such as ash and tar are produced during the transformation of feedstocks (Calijuri et al., 2022). Moreover, the conversion of aquatic biomass (e.g., microalgae, sewage sludge) via high-temperature atmospheric processes is a challenging task due to the high moisture content of these feedstocks (up to even 80–90% (Islam et al., 2022)) and the requirement of energy-intensive pre-drying steps (Min et al., 2022). As a bypass solution, sub-, or supercritical water-based technologies can be applied to convert raw biogenic materials using their own water content as a reagent and solvent and to produce solid hydrochar (Liu et al., 2022), liquid bio-oil (Adedeji et al., 2022), hydrogen-rich fuel gas mixtures (Rajagopal et al., 2022) and subsequently, value-added chemical products such as methanol (Fózer et al., 2021).

Hydrothermal carbonisation was applied to produce mainly hydrochar (with solid yields up to 50–80%) by using various feedstocks such as aquatic biomass (*Chlorella vulgaris*, *Didymocystis inermis*, *Tetradesnus obliquus*) (de Siqueira Castro et al., 2021), waste (Xu et al., 2021) and plastic (Iñiguez et al., 2019). Khoo et al. (2020) produced an energy-dense hydrochar from *Chlorella vulgaris* microalgae by optimising HTC reaction temperature and retention time parameters. Climate change benefits of the HTC process were reported to be sufficient to outweigh the impacts of production in cases where the stability of hydrochar is adequately high for storage purposes (Owsianiak et al., 2018). However, Zhang et al. (2021) highlighted the need to improve process efficiencies and economic costs of hydrothermal carbonisation and suggested the recovery of value-added products from the reaction media.

Producing hydrogen from microalgae by thermochemical technologies could result in favourable carbon emission footprints; however, the non-catalytic hydrothermal and atmospheric transformation of aquatic biomass require high reaction temperatures and a high amount of energy to achieve elevated gasification efficiencies (Tiong and Komiyama, 2022). This limitation makes it necessary to apply (1) catalysts (Xie et al., 2019), (2) co-gasifying agents (Huang et al., 2018), (3) enhanced energy recovery (Behera et al., 2022) or (4) various mediators (Zhang et al., 2021) to improve conversion efficiencies, hydrogen yield, product characteristics, and environmental performances. Acid-mediated sub-critical treatments offer a simple and attractive way to improve the hydrothermal conversion and characteristics of HTC-derived biofuels (Sarrion et al., 2022). Evcil et al. (2020) investigated the use of combined Lewis and Brønsted acids ($AlCl_3$-HCl) on lignocellulosic biomass. They observed that the catalyst combination decreased hydrochar yield and increased the heating value up to 29.19 MJ kg^{-1} at 275 °C and 24 h residence time. Lachos-Perez et al. (2022) discussed that intermediate products (e.g., acetic acid and formic acid) formed during the HTC process could affect the HTC gas composition and enhance the formation of CO_2 and minor gases. Lu et al. (2022) showed that formic acid decreases the content of nitrogen heterocyclic compounds in the produced bio-oil. Wang et al. (2018) highlighted that HTC liquid and gas products have received limited research attention and also pointed out the need for advanced reaction modelling to guide the development of HTC-based technologies.

Modelling hydrothermal processes are challenging due to the unclear reaction mechanisms and the high number of parallelly occurring reactions that require simplifications in kinetic simulations (Yang et al., 2022). Machine learning (ML) algorithms (e.g., artificial neural networks) provide a framework for simulating complex chemical processes without knowing exact reaction kinetics using a black-box approach. ML was already applied to simulate the production of biochar (Zhu et al., 2019), the co-pyrolysis of sewage sludge (Bi et al., 2021) or to predict the viscosity of slurry in the hydrothermal hydrolysis process (Chen et al., 2021). However, there is a lack of research on models development that involve the use of mediators and focus on the evolution of the gas phase in low-temperature hydrothermal processes.

Former hydrothermal carbonisation studies focused mainly on improving the yield and properties of hydrochar. The main goals of this work are to *(i)* assess the gas formation and green hydrogen production potentials of hydrothermal carbonisation using *Chlorella vulgaris*, a model microalgae biomass, and *(ii)* develop an accurate artificial neural network to describe gas formation under acid-mediated sub-critical conditions. The present study shows that formic acid-mediated hydrothermal carbonisation of microalgae biomass can boost HTC gas formation, and the obtained green hydrogen yield competes with other thermochemical technologies (e.g., hydrothermal gasification and pyrolysis).

2. Materials and methods

2.1. Materials

Chlorella vulgaris (*C. vulgaris*) microalgae feedstock was acquired from the commercial market (Vital-Trend Kft., Hungary) in dried form. The proximate analysis of *C. vulgaris* showed that the volatile matter, fixed carbon and ash content of the dried biomass are 84.14 wt.%, 10.70 wt.% and 5.16 wt.%, respectively. The elemental composition of *C. vulgaris* was calculated based on the work of Parikh et al. (2007). The investigated microalgae strain contained 45.10 wt.% C, 5.77 wt.% H, 43.30 wt.% O, and 5.82 wt.% N. The higher heating value of the dried *C. vulgaris* was 18.01 MJ $(kg)^{-1}$. Acetone (⩾99.5%) and formic acid (⩾95%) were purchased from Merck KGaA, Germany.

2.2. Experimental procedure

2.2.1. Hydrothermal carbonisation

Autogenous hydrothermal carbonisation was carried out in a 250 mL batch autoclave reactor (MT-07300, Parr Instrument Company, USA). Inert atmosphere was provided by washing the reactor vessel with nitrogen. A Heidolph MR 3003 control magnetic stirrer with a hotplate was applied for heating the reactor that was insulated using rockwool. The biogas was collected in a gas burette (2,000 mL) and sampled using a septum attachment. The solid and liquid phases were separated with a Hettich Rotina 380 1701 centrifuge by using 3,758 relative centrifugal force (G-force) separation and sedimentation performance for 5 min. The synthesised hydrochar was dried for constant weight at 105 °C using a drying cabinet (Heraeus D-6450 Hanau).

2.2.2. Analysis of solid hydrochar and C. vulgaris

The proximate analysis of hydrochar samples was performed based on the ASTM D3175 (volatile matter, VM), ASTM D3174 (ash) and ASTM D3172 (fixed carbon, FC) standards. The VM was determined by igniting the samples at 950 °C for 7 min in a platinum crucible. The ash content of HC samples was measured by heating them in ceramic crucibles to 500 °C and 950 °C using 8.3 and 7.5 °C min^{-1} heating rates, respectively. Then, the samples were ignited at 950 °C for 2 h. The FC content was determined by Eq. 1:

$$FC\,(wt.\%) = 100 - VM - ash. \quad (1)$$

The thermogravimetric analysis (TGA) of *Chlorella vulgaris* feedstock was carried out using a Perkin Elmer STA-6000 device. The dried microalgae samples (approximately 10 mg) were heated in an alumina crucible from room temperature to 950 °C using four different heating rate settings: 2; 5; 10; and 20 K min^{-1}. Inert atmosphere was applied

during the measurements; the nitrogen flow rate was set to 20 mL min^{-1}.

2.2.3. Analysis of gaseous products

The HTC gas samples were measured with an HP5890A Series II gas chromatograph equipped with thermal conductivity and flame ionisation detectors. A 1.9 m × 3.175 mm (LxØ) packed column (filled with Porapak Q, 80–100 mesh load) was utilised for the separation of gas components. The initial temperature of the oven was set to 50 °C for 30 s. The oven temperature was increased to 150 °C using 20 °C min^{-1}heating rate. The column head pressure of argon carrier gas was 150 kPa.

2.2.4. Analysis of liquid products

The co-produced process water was analysed using a Shimadzu GC/MS-QP2010 SE gas chromatograph mass spectrometer. The process water was filtered using a syringe filter (hydrophilic PTFE, 0.45 µm, FilterBio®). 0.1 mL sample was diluted in 0.9 mL acetone. The injector temperature was 280 °C, the ion source and interface temperatures were set to 250 °C and 290 °C. The initial temperature was 40 °C, which was held for 1 min. Then, the temperature was increased to 150 °C using 5 °C min^{-1} heating rate. Finally, the oven temperature was raised to 320 °C using 10 °C min^{-1} heating rate and was held for 5 min. The He flow rate in the column was 1.2 mL min^{-1}, the split ratio was set to 3. The mass spectrometer was operated at an m/z scan range of 50–650. SGE BP5 (25 m x 0.25 mm ID) capillary column was used for the separation of compounds.

Shimadzu TOC-VCSN analyser was used to measure the total carbon, inorganic carbon and total organic carbon contents of process water samples.

2.3. Data analysis

The hydrochar yield (Y_{HC}, %) was determined using Eq. 2:

$$Y_{HC}\,(\%) = \frac{\text{mass of dried hydrochar (g)}}{\text{mass of dried microalgae (g)}} \cdot 100\%, \tag{2}$$

The higher heating value of the produced solid fuel samples (HHV_{SF}, MJ kg^{-1}, $R^2 = 0.9597$, Eq. 3) was determined using an empirical formula reported by Dashti et al. (2019):

$$\begin{aligned} HHV_{SF}\left(MJ\ kg^{-1}\right) = \; & -0.0038\left(-19.9812FC^{1.2259} - 1.0298\cdot10^{-13}VM^{8.0664} + \right. \\ & +0.1026Ash^{2.4231} - 1.2065\cdot10^{-7}\left(FC\cdot Ash^{4.6653}\right) + 0.0228\left(FC\cdot VM\cdot Ash\right) - \\ & \left. -0.2511(VM/Ash)\right) - 0.0478(FC/VM) + 15.7199 \end{aligned} \tag{3}$$

The energy densification (ED, -) and fuel ratio (FR, -) were calculated by Eq. 4 and 5:

$$ED\,(-) = \frac{HHV_{HC}}{HHV_{feedstock}}, \tag{4}$$

$$FR\,(-) = \frac{FC}{VM}, \tag{5}$$

where HHV_{HC} and $HHV_{feedstock}$ are the higher heating value (MJ kg^{-1}) of hydrochar and microalgae feedstock, FC and VM are the fixed carbon and volatile matter contents (wt.%).

The energy (η_{ER}, –)-, and fixed carbon recovery efficiencies (η_{FCR}, –) were obtained according to Eq. 6 and 7:

$$\eta_{ER}\,(-) = \frac{HHV_{HC}}{HHV_{feedstock}} \cdot \frac{Y_{HC}}{100\%}, \tag{6}$$

$$\eta_{FCR}\,(-) = \frac{FC_{HC}}{FC_{feedstock}} \cdot \frac{Y_{HC}}{100\%}. \tag{7}$$

The biogas yield (Y_{biogas}, $mol\ kg^{-1}$) was determined based on Eq. 8:

$$Y_{biogas}\left(mol\ kg^{-1}\right) = \frac{\sum\left(n_{GAS,i}\right)}{m_{feedstock}} \qquad i = H_2, CH_4, CO_2, CO, C_2H_4, C_2H_6, \tag{8}$$

where $n_{GAS,i}$ is the mole number of the i^{th} gas component (mol), $m_{feedstock}$ is the mass of the feedstock (kg).

The carbon gasification efficiency (CGE, -) was determined by Eq. 9:

$$CGE\,(-) = \frac{\sum\left(n_{GAS,j}\cdot\frac{MW_C}{MW_{GAS,j}}\right)}{m_{feedstock}\cdot\frac{x_{feedstock,C}}{MW_C}} \qquad j = CH_4, CO_2, CO, C_2H_4, C_2H_6, \tag{9}$$

where MW_C and $MW_{GAS,j}$ are the molecular weight of carbon and the j^{th} gas component (g mol^{-1}), $x_{feedstock,C}$ is the mass fraction of carbon in the feedstock (–). The hydrogen gasification efficiency (HGE, -) was calculated based on Eq. 10:

$$HGE\,(-) = \frac{n_{H_2}}{m_{feedstock}\cdot\frac{x_{feedstock,H}}{MW_H}} \tag{10}$$

where n_{H_2} is the mole number of H_2 (mol), $x_{feedstock,H}$ is the mass fraction of hydrogen in the feedstock (–), MW_H is the molecular weight of hydrogen (g mol^{-1}).

The effectiveness of the hydrothermal treatment was evaluated by the severity factor ($\log_{10}R_0$) (Morales-Contreras et al., 2022). The severity factor, defined as the logarithm of reaction ordinate (R_0), combines reaction temperature and time into one variable using the Arrhenius Law. The reaction ordinate is expressed in Eq. 11:

$$R_0\,(min) = \int_0^{\tau} exp\left(\frac{T_r - T_b}{\left(\frac{T_f^2 R}{E_a}\right)}\right) dt, \tag{11}$$

where T_r is the reaction temperature (°C), T_b is the base temperature (°C) (assumed to be 100 °C), T_f is the "floor" temperature equal to the central level of the applied reaction temperature range (°C), R is the universal gas constant (8.314 J $K^{-1}mol^{-1}$), E_a is the activation energy (J mol^{-1}), τ is the reaction time (min) (i.e., the sum of residence time and the time that is required to reach the reaction temperature from the base temperature). The severity factor was modified to include the effects of using acid mediators in different concentrations assuming a first-order reaction rate (Chen et al., 2007) and named as the combined severity factor (CSF, Eq. 12) (Chum et al., 1990):

$$CSF(-) = lg(R_0) - pH \quad (12)$$

The Kissinger equation (expressed in Eq. 13) was used to determine the apparent activation energy and pre-exponential constant (A) based on thermogravimetric analysis (Vyazovkin et al., 2011):

$$ln\left(\frac{\beta}{T_{m,i}^2}\right) = ln\left(-\frac{AR}{E_a}\frac{d(1-\alpha)}{d\alpha}\right) - \frac{E_a}{RT_{m,i}}, \quad (13)$$

where α is the extent of conversion (–), β is the heating rate (K min^{-1}).

2.4. Artificial neural network (ANN) modelling

The formic acid-mediated hydrothermal carbonisation of *Chlorella vulgaris* biomass was modelled by developing a multi-input and multi-output artificial neural network using the MATLAB R2021a software (MathWorks, 2021). Bayesian regularisation algorithm was used for training because of its ability to reach good generalisation with small datasets, it is difficult to overtrain or overfit, and it does not require lengthy cross-validation (Burden and Winkler, 2009). The input data is based on a 3-factorial central composite design of experiments (generated using the HTC reaction temperature, feedstock-to-suspension ratio and catalyst-to-suspension ratio) that is expanded up to 30 cases by adding entries between low and high factor levels. The reaction temperature, reaction time and pH variables were transformed into the combined severity factor. Machine learning models were trained using the combined severity factor and the feedstock-to-suspension ratio. Input data (detailed in Table 1) were randomly assigned between the training (80%) and testing (20%) stages. The input data was pre-processed before model training by using z-score (z, -) normalisation as shown in Eq. 14:

$$z\left(-\right) = \frac{\mu - \overline{\mu}}{SD} \quad (14)$$

where μ is the sample value, $\overline{\mu}$ is the mean value of the sample data, SD is the standard deviation.

The target variables were divided into three categories based on HTC product phases:

- solid phase: (i) hydrochar yield (%); (ii) volatile matter (wt.%); (iii) fixed carbon (wt.%); and (iv) ash content (wt.%),
- liquid phase: (i) total organic carbon content (mg L^{-1}),
- gaseous phase: (i) hydrogen yield (mol kg^{-1}); (ii) methane yield (mol kg^{-1}); (iii) carbon dioxide yield (mol kg^{-1}); (iv) carbon monoxide yield (mol kg^{-1}); (v) ethylene yield (mol kg^{-1}); and (vi) ethane yield (mol kg^{-1}).

The training and testing performances of neural network topologies were evaluated based on the mean squared error (MSE_z) (Eq. 15). The accuracy of ANN models was tested by the coefficient of determination (Eq. 16).

$$MSE_z = \frac{\sum_{j=1}^{n}\left(Y_{pred,j}^z - Y_{exp,j}^z\right)^2}{n}, \quad (15)$$

$$R_z^2 = 1 - \frac{\sum_{j=1}^{n}\left(Y_{pred,j}^z - Y_{exp,j}^z\right)^2}{\sum_{j=1}^{n}\left(Y_{exp,j}^z - \overline{Y}_{exp,j}^z\right)^2}, \quad (16)$$

where $Y_{pred,j}^z$ is the predicted, $Y_{exp,j}^z$ is the experimental, $\overline{Y}_{exp,j}$ is the average of all factor level(s) of the z^{th} target variable, and n is the number of data.

3. Results and discussion

3.1. Determining kinetic constants for assessing hydrothermal reaction severity

The TGA experimental results of *Chlorella vulgaris* biomass are shown in Figs. 1a to 1d. Combusting the dried feedstock using distinct 2–20 K min^{-1} heating rate levels resulted in one major low peak on the corresponding derivative thermogravimetric (DTG) curves. The peaks indicate a combustion process between 200 °C and 500 °C that is attributed to the combustion and evaporation of volatiles. Similar combustion characteristics were reported by Ye et al. (2020), who investigated the co-combustion of coal and microalgae. The temperature values at the extrema of DTG curves are used to formulate a linear function, as is presented in Fig. 1e. The Kissinger equation, constructed based on thermogravimetric analysis measurements and DTG curves, is expressed in Eq. 17 (R^2=0.9717).

$$ln\left(\frac{\beta}{T_{max}^2}\right) = -15,923\left(\frac{1}{T_{max}}\right) + 11.688 \quad (17)$$

Based on the Kissinger equation, kinetic constants are calculated and used to determine the severity factor. It is obtained that the apparent activation energy and pre-exponential constant of the dried *Chlorella vulgaris* biomass is 132.4 ± 1.9 kJ mol^{-1} and 1.896E+09 ± 2.683E+07 s^{-1}. These results are in agreement with the findings of Soria-Verdugo et al. (2018) who reported the activation energy and pre-exponential constant of *Chlorella vulgaris* microalgae strain in a range of 135.6–337.1 kJ mol^{-1} and 8.7E+09–4.1E+21 s^{-1}, respectively.

3.2. Artificial neural network (ANN) modelling

The experimental results of non-catalysed and formic acid-mediated hydrothermal carbonisation of *Chlorella vulgaris* are summarised in Table 1. Supervised machine learning models are developed based on experimental data and used to model the hydrothermal conversion in a wide range of combined reaction severity [-2.5, 2.9] and feedstock-to-suspension ratio [5 wt.%, 25 wt.%] intervals. It is obtained that the number of hidden layers and hidden neurons significantly influences the performance of neural networks. The training and testing performances and accuracies are fine-tuned by examining one and two hidden layer topologies and adjusting the number of hidden neurons from 5 to 20. A total of 272 neural network topologies are developed and trained (see supplementary material). Neural network topologies with one hidden layer resulted in adequate training accuracies ($R^2 \geqslant 0.974$); however, the testing coefficients of determination were less accurate with values ranging between 0.833 and 0.942. The underfitting is explained by the insufficient level of resolving complex correlations between input and target variables. The simulation results show that adding one additional hidden layer to the perceptron enables to obtain better accuracies in many of the investigated neural net scenarios. The ideal neural network topology (BR-2-11-9-11) consisting of two hidden layers is illustrated in Fig. 2a. The best model training (R^2= 0.9974, Fig. 2b) and testing (R^2= 0.9781, Fig. 2c) accuracies are achieved with 11 neurons in the first and 9 neurons in the second hidden layer. The BR-2-11-9-11 multi-layer perceptron is characterised by low training and the lowest testing errors with MSE_zvalues of 1.71E-06 and 1.40E-06. Increased mean squared errors are observed when the number of hidden neurons raised above ideal values. This tendency indicates that the modelling performance reached its peak with the given training set, and the performance could be increased only by expanding the size of the input database using more complex ANN topologies that contain surplus hidden neurons, or reducing the complexity of the multi-layer perceptron by decreasing the number of input variables. Thus, the obtained BR-2-11-9-11 perceptron is identified as the best neural network topology for the available HTC measurements-based input dataset. These results shows the benefits of

Table 1
Experimental set-up and results of formic acid-mediated hydrothermal carbonisation.

No	Experimental parameters						Hydrochar characteristics				TOC (mg L^{-1})	Biogas yield and composition						
	T (°C)	τ(min)	pH (–)	CSR (wt. %)	CSF (–)	FSR (wt. %)	Y_{HC} (%)	VM (wt. %)	FC (wt. %)	Ash (wt. %)		Y_{GAS}(mol kg^{-1})	H_2(mol %)	CH_4(mol %)	CO_2(mol %)	CO (mol %)	C_2H_4(mol %)	C_2H_6(mol %)
1	180	67	5.38	0	−1.081	12.5	46.7	87.1	9.5	3.4	29,790	0.38	0.45	0.25	94.15	5.13	2.97E-03	8.01E-03
2	220	142	7.86	0	−1.999	12.5	27.7	82.4	12.3	5.3	33,970	1.67	0.12	0.12	96.43	3.28	1.53E-02	3.33E-02
3	180	76	2.76	10	1.594	12.5	27.7	85.4	12.4	2.2	59,440	2.95	16.61	0.03	80.69	2.66	2.05E-03	3.63E-03
4	220	130	3.39	10	2.433	12.5	5.1	77.5	13.7	8.8	50,600	13.42	22.63	0.02	71.76	5.57	5.59E-03	4.69E-03
5	180	79	2.60	5	1.770	5.0	25.4	88.1	10.1	1.8	27,290	1.60	2.89	0.03	91.18	5.89	2.01E-03	5.89E-03
6	220	146	2.93	5	2.943	5.0	10.5	87.8	10.8	1.4	24,940	7.70	16.87	0.03	81.20	1.89	6.30E-03	5.68E-03
7	180	94	3.39	5	1.056	20.0	37.7	87.0	10.3	2.8	62,240	2.56	1.70	0.03	95.89	2.37	2.88E-03	8.18E-03
8	220	157	5.26	5	0.645	20.0	17.3	83.8	10.2	6.0	63,670	6.46	3.47	0.02	91.21	5.28	8.03E-03	8.66E-03
9	200	105	5.66	0	−0.550	5.0	32.0	83.1	13.4	3.5	14,080	1.09	0.23	0.08	96.64	3.04	5.47E-03	1.17E-02
10	200	109	2.41	10	2.716	5.0	13.2	83.3	15.7	1.0	38,440	4.68	11.62	0.03	85.83	2.51	2.89E-03	5.67E-03
11	200	120	6.40	0	−1.232	20.0	41.6	85.2	9.6	5.3	52,400	1.60	0.67	0.03	96.19	3.08	7.42E-03	1.81E-02
12	200	123	3.37	10	1.809	20.0	15.6	84.1	13.8	2.1	75,150	5.92	2.75	0.02	88.53	8.69	4.75E-03	5.07E-03
13	200	102	3.28	5	1.817	12.5	22.2	87.1	11.7	1.2	45,050	3.98	1.23	0.02	96.48	2.25	2.85E-03	4.58E-03
14	200	104	3.29	5	1.816	12.5	19.4	87.1	11.3	1.6	45,180	4.16	0.58	0.02	95.74	3.66	1.86E-03	4.02E-03
15	200	103	3.31	5	1.792	12.5	21.3	88.6	10.3	1.1	51,690	4.17	2.17	0.03	95.49	2.30	3.15E-03	6.13E-03
16	220	99	6.77	0	−1.066	15.0	17.1	71.8	20.9	7.4	38,720	2.56	0.02	0.13	97.04	2.76	5.27E-03	3.71E-02
17	180	80	5.13	0	−0.754	5.0	29.2	83.0	14.4	2.6	14,480	0.51	0.03	0.12	95.80	4.02	2.24E-03	3.71E-02
18	200	86	5.80	0	−0.772	25.0	30.7	73.3	20.8	5.9	54,690	1.90	0.05	0.12	83.58	16.21	6.11E-03	3.03E-02
19	180	92	6.72	0	−2.283	7.5	30.5	89.6	5.7	4.8	24,740	0.96	0.02	0.03	92.93	7.02	9.00E-03	4.00E-03
20	220	107	8.20	0	−2.462	7.5	13.5	83.3	8.6	8.1	26,350	1.58	0.01	0.05	97.12	2.78	2.00E-02	1.00E-02
21	180	93	6.97	0	−2.529	15.0	38.5	86.9	6.1	7.0	47,060	1.27	0.06	0.04	91.11	8.77	1.30E-02	1.00E-02
22	220	103	8.24	0	−2.518	15.0	16.3	79.9	10.6	9.5	46,650	2.56	0.10	0.04	95.99	3.83	1.70E-02	1.90E-02
23	190	129	3.65	2.5	1.242	15.0	38.1	88.2	9.1	2.7	37,980	2.59	1.21	0.04	95.29	3.45	3.69E-03	6.66E-03
24	210	100	3.31	2.5	2.090	7.5	23.3	84.5	12.7	2.8	23,600	3.56	4.45	0.04	92.27	3.22	6.32E-03	6.77E-03
25	220	120	3.11	7.5	2.678	12.5	10.9	89.5	10.0	0.5	43,690	8.01	8.03	0.03	88.84	3.10	6.00E-03	4.54E-03
26	180	78	2.44	7.5	1.925	7.5	26.7	85.8	12.8	1.4	36,140	1.76	0.45	0.03	95.70	3.81	1.06E-03	4.97E-03
27	200	94	5.00	1	0.064	20.0	41.5	83.6	10.2	6.2	42,570	2.40	0.47	0.06	96.56	2.90	4.37E-03	1.01E-02
28	180	130	2.94	9	1.647	17.5	29.2	86.6	9.8	3.6	56,150	3.84	12.63	0.04	83.86	3.46	2.97E-03	4.06E-03
29	180	121	2.69	10	1.866	12.5	30.7	80.9	12.9	6.3	49,410	4.01	23.41	0.06	73.97	2.55	3.92E-03	6.40E-03
30	210	99	6.03	0	−0.634	5.0	32.7	82.5	13.6	3.9	13,420	1.22	0.15	0.12	96.99	2.72	1.00E-02	1.53E-02

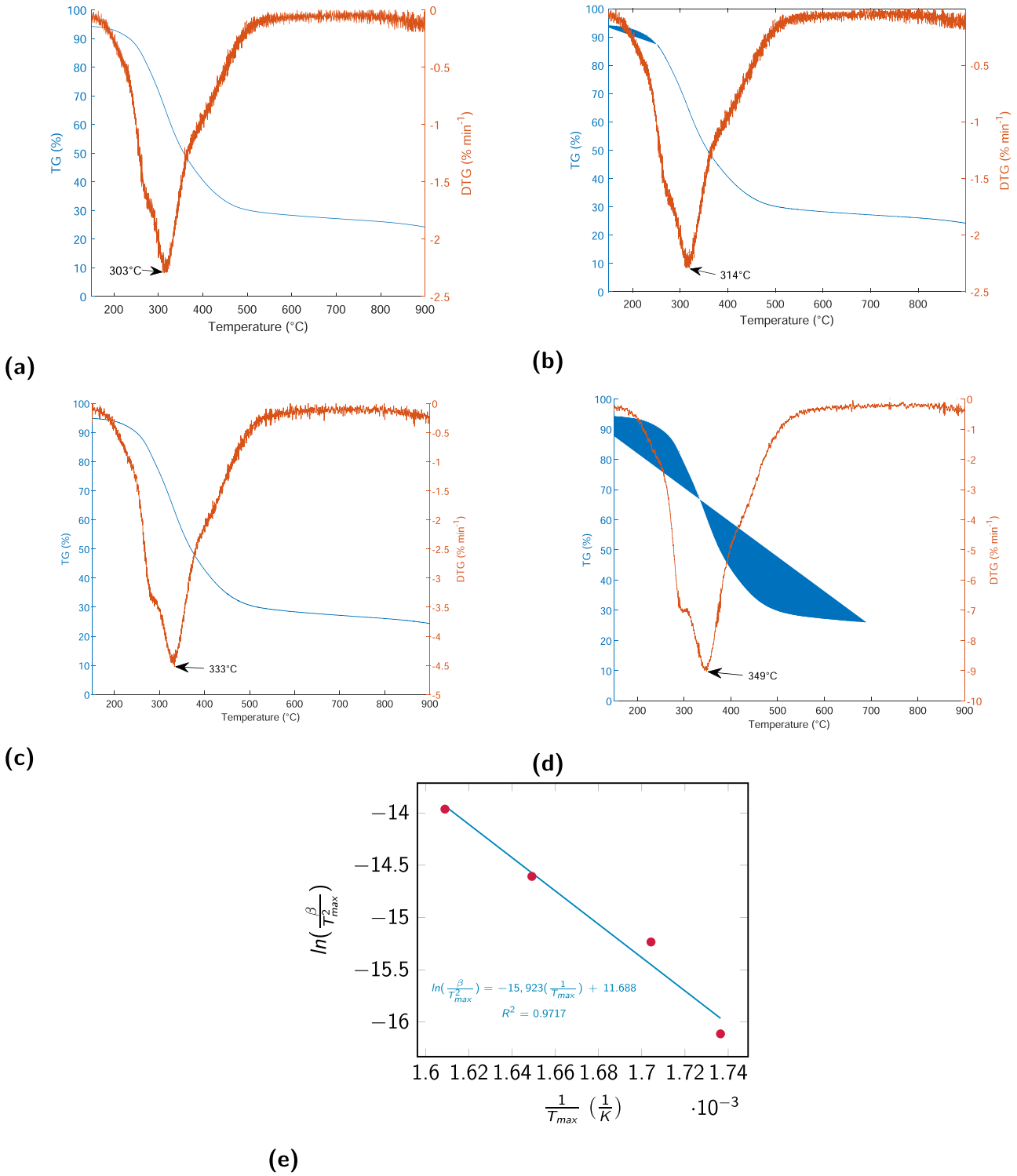

Fig. 1. TG and DTG curves of *Chlorella vulgaris* microalgae feedstock obtained at different heating rates: (a) 2 K min^{-1}, (b) 5 K min^{-1}, (c) 10 K min^{-1}, (d) 20 K min^{-1}; and (e) the obtained Kissinger equation costructed based on TGA measurements.

using the combined severity factor from modelling point of view. The utilisation of the CSF parameter that combines the HTC reaction temperature, reaction time and pH factors into one variable enables the reduction of the number of input variables, the complexity of ANN structures and the size of the required input dataset facilitating the development of high performing and accurate ML models.

Complying with computational rigour requires a detailed description of model assumptions and limitations. The major assumptions and limitations of the developed machine learning-based HTC model are discussed below:

- The experimental dataset and applied apparatus ultimately influence the capabilities of the model. The ML model is best suited to describe the hydrothermal conversion of aquatic biomass in batch-type autoclaves that are operated below 250 °C and apply an autogenic

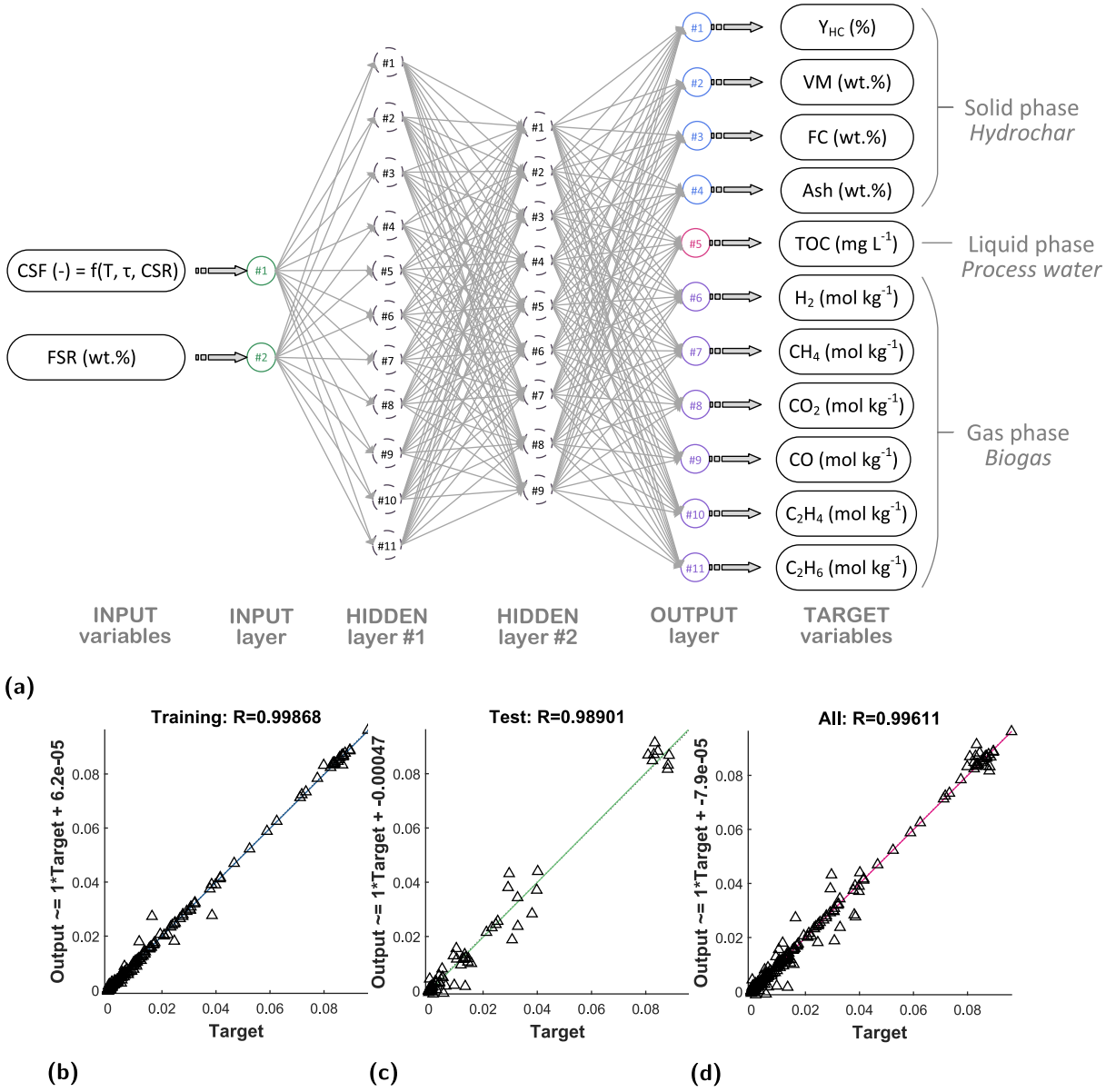

Fig. 2. The ideal topology of the artificial neural network, training & testing. The characteristics of artificial neural networks used for the modelling of formic acid-mediated hydrothermal carbonisation. (a) ideal BR-2-11-9-11 ANN topology, (b) training accuracy, (c) testing accuracy, (d) combined coefficient of correlation.

pressure regime and nitrogen atmosphere during the sub-critical reaction.

- The model adequately describes the non-catalytic and formic acid-mediated hydrothermal carbonisation of *Chlorella vulgaris* feedstock; however, it may provide less accurate results when other microalgae strains or biomass types are in the centre of interest.
- The trained model is applicable in a combined severity factor and feedstock-to-suspension ratio intervals of −2.5 and 2.9; and 5 wt.% - 25 wt.%.
- The applied GC/TCD/FID analytical system was able to detect hydrogen, methane, carbon dioxide, carbon monoxide, ethylene, and ethane in HTC gas samples. Thus, it is assumed that the produced gas mixture contains mainly these compounds.

3.3. The effects of combined severity factor and feedstock concentration on hydrochar formation

The results show that the combination of elevated temperature levels and the use of formic acid decreases the hydrochar yield. Y_{HC} is reduced by 40.8% from 46.7% by employing acid mediation at 10 wt.% CSR, 180 °C and 12.5 wt.% FSR. Conducting hydrothermal carbonisation at elevated temperature (220 °C) and reaction time (142 min) settings resulted in similar hydrochar yield reduction (40.6%). Combined high factor levels (i.e., $T_{r,HTC}$= 220 °C, τ = 130 min, CSR = 10 wt.% at 12.5 wt.% FSR) reduced the hydrochar yield to 5.1%. It is observed that using harsher hydrothermal carbonisation regimes can elevate the total gas yield and the TOC content of the HTC liquid to 13.42 mol kg^{-1} and 50,600 mg L^{-1}. These results indicate that applying enhanced reaction severities (e.g., a CSF of 2.433) shifts product formation from the solid phase toward volatile liquids and gaseous compounds.

The hydrochar yield is illustrated as a function of the combined severity factor and feedstock-to-suspension ratio in Fig. 3a. It is obtained that lower severity (CSF ⩽0) and feedstock concentration (FSR ⩽13 wt.%) levels are preferred to strengthen hydrochar formation. Positive CSF levels were attained by using formic acid mediation; thus, the ML model confirms that formic acid-based treatment has a negative effect on the HC yield. This finding is in agreement with the TOC analysis of the liquid phase. Fig. 3b demonstrates that the total organic carbon content rises

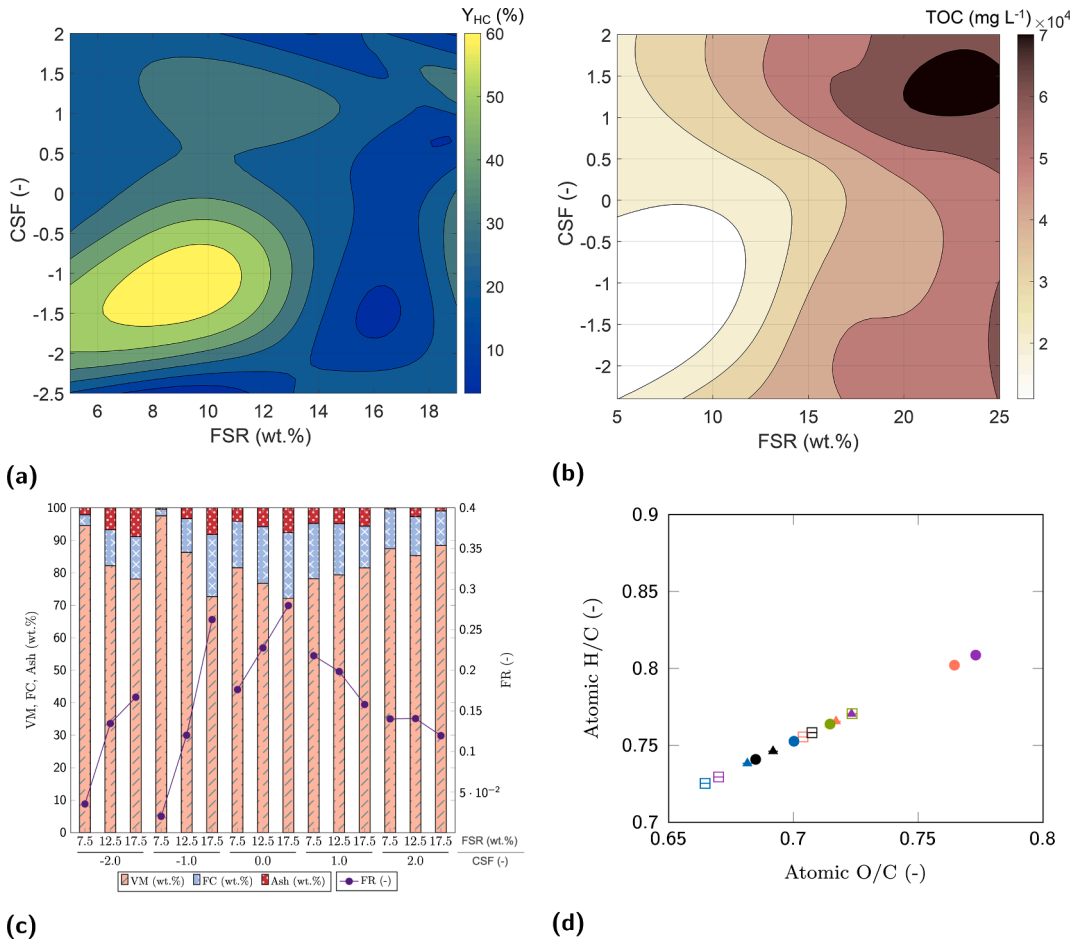

Fig. 3. Hydrochar composition and properties. a.) the effects of CSF and FSR on the hydrochar yield; b.) on the total organic carbon content of the liquid product phase; c.) the composition and fuel ratio of hydrochar; d.) Van Krevelen diagram, marks indicate feedstock-to-suspension ratios (i.e., 7.5 wt.%: circles (●, ●, ●, ●, ●), 12.5 wt.%: triangles (▲, ▲, ▲, ▲, ▲), 17.5 wt.%: squares (□, □, □, □, □)), colours indicate the levels of combined severity factor (CSF=-2: pale red, CSF=-1: purple, CSF = 0: blue, CSF = 1: black, CSF =;2: applegreen).

significantly as the CSF and FSR levels increase. It is observed that the TOC content of process water is the lowest in those specific combined severity factor and FSR intervals where hydrochar formation occurs at the highest intensity (-2.5 < CSF <0; 5 wt.% < FSR <13 wt.%). These results display that the formic acid-boosted hydrothermal conversion enhances the formation of volatile compounds at increased CSF levels. In this way, acid mediation and the targeted use of combined reaction severities improve the flexibility of hydrothermal pretreatments. Depending on biomass valorisation scenarios (e.g., H_2 for Power-to-X applications, or high-quality secondary hydrochar fuel for rotary

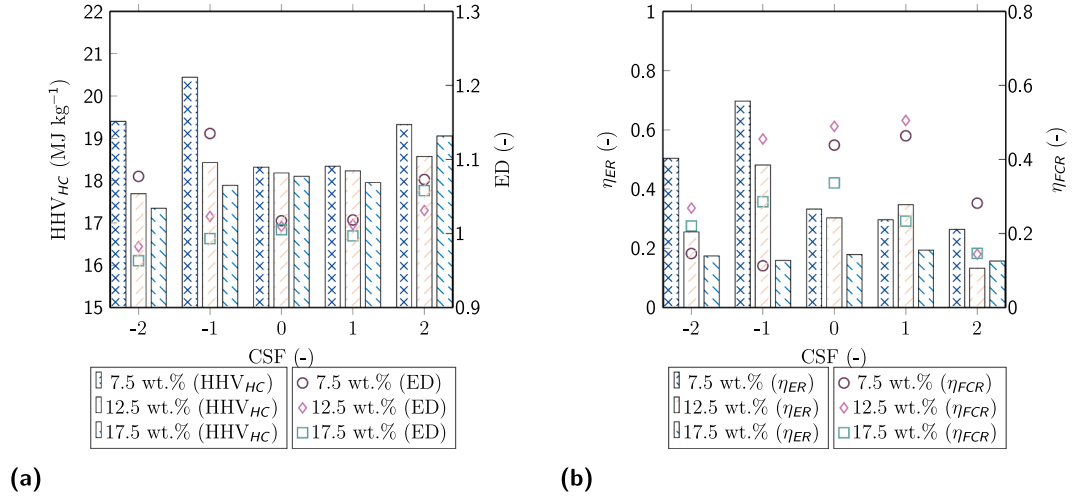

Fig. 4. The effects of combined severity factor and feedstock-to-suspension ratio on the (a) higher heating value of hydrochar, energy densification of hydrothermal carbonisation, and (b) energy- and fixed carbon recovery efficiencies.

kilns), the biomass pretreatment step can be fitted to preferred end-use cases by shifting the production rate between solid, liquid and gaseous fractions.

Fig. 3c shows the proximate composition and fuel ratio of hydrochar produced using various combined severities and feedstock concentration. A tendency difference is observed between positive and negative CSF reaction conditions. Raising microalgae concentration contributes to achieving higher fuel ratios and product stability when negative or zero severities are applied. On the other hand, lower FSR levels are preferred in positive CSF scenarios. The results demonstrate that harsher hydrothermal severity condition (CSF $\geqslant$0) reduces the fuel ratio of hydrochar. There is a link between the fuel ratio and stability of solid fuels (Leng et al., 2019); thus, the results indicate that formic acid-assisted cases lower the stability of solid combustible hydrochars. The decreased stability is also confirmed by illustrating the atomic composition of HC samples on a van Krevelen diagram (Fig. 3d). The diagram shows that increased combined severity (CSF = 2, indicated with apple green colour) slightly reduces the degree of coalification (H/C and O/C ratios) of hydrochar. Better dehydrogenation and reduction were achieved by applying CSF regimes between −1 and 1 (highlighted with purple, blue and black colours). Low combined severity factor level (-2, pale red) was not favoured for the coalification of microalgae. Thus, the formic acid-mediated hydrothermal carbonisation results in elevated green hydrogen production at the cost of reduced stability of hydrochar. This finding indicates that the acid-mediated hydrochar is better suited for short-term applications (e.g., as a secondary fuel) rather than as a long-term (more than 10–100 years) carbon storage material.

The energy densification and higher heating value of hydrochars are presented in Fig. 4a. Increasing the combined severity from −2 to −1 is found to be beneficial in improving energy densification (up to 1.14 at CSF=-1) and the heating value (20.44 MJ kg^{-1} at CSF=-1) of microalgae-derived solid fuels. A considerable drop (-10.4%) is observed in the value of ED and HHV_{HC} by elevating the hydrothermal reaction severity up to zero. The results indicate that the feedstock-to-suspension ratio plays an important role in attaining better energy densification and calorific values. It is obtained that the higher heating value of hydrochar can be increased from 17.3 MJ kg^{-1} to 19.4 MJ kg^{-1} by lowering the feedstock concentration from 17.5 wt.% to 7.5 wt.%. The hydrochar energy conversion and fixed carbon recovery efficiencies are illustrated in Fig. 4b. The energy conversion efficiency shows similar tendencies to the higher heating value of HC. η_{ER} decreases at higher FSR and CSF >0 levels. The fixed carbon recovery efficiency improves when the CSF is increased above 0 and peaks at CSF = 1. This result confirms that high hydrothermal severities (CSF >1) increase the formation of carbon-rich volatile compounds.

3.4. GC–MS analysis of HTC liquid phase

The GC–MS spectra of the liquid phase were analysed to quantify the peak areas of detected compounds and to compare relative content changes using different hydrothermal reaction conditions. Liquid products were classified into aliphatic hydrocarbons, alcohols, aldehydes, ketones, acids, heterocyclic compounds, esters, aromatic and N–heteroatom compounds. The composition of organics in HTC process water samples is shown in Fig. 5. The results show that the combined reaction severity influences the composition of organics in the liquid phase product. Positive CSF conditions yielded HTC liquid samples containing mainly acids, esters, heterocyclic and N–heteroatom compounds. Higher hydrothermal severity (CSF >0) increased the acid composition of organics above 50%. Liu et al. (2022) reported that the removal of ketones and aromatics was increased by treating the aqueous phase of hydrothermal carbonisation with potassium persulfate. Similar results are obtained *in situ* via formic acid-assisted hydrothermal carbonisation, where the amount of ketones, heterocyclic and aromatic compounds is reduced at elevated hydrothermal reaction severity levels (CSF >0). Liu et al. (2022) discussed that the presence of aromatics plays an important role in hydrochar formation contributing to the production of carbonaceous microspheres with stable oxygen groups, and increased acidity of the aqueous phase may affect deoxygenation reactions and the quality of hydrochar. The results show that hydrotreating *Chlorella vulgaris* at low severities (CSF <0) increases the amount of aromatic and heterocyclic compounds in the liquid phase. Simultaneously, hydrochar samples are obtained to be more stable (with a higher fuel ratio) by conducting experiments at negative combined severity regions (Fig. 3). Therefore, increasing reaction severity reduces hydrochar stability (Fig. 3c), raises the formation of volatile compounds (Fig. 3b) and the

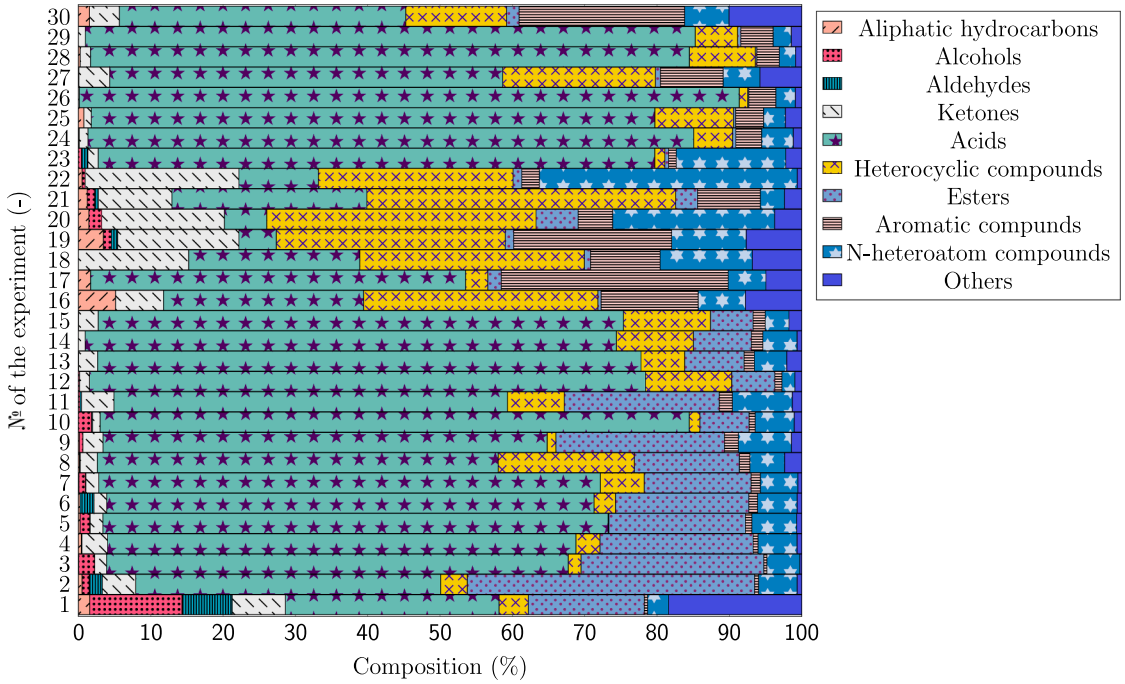

Fig. 5. Content distribution of main products in the HTC process water.

acidity of the aqueous phase (3^{rd}-8^{th}; 10^{th}; 12^{th}-15^{th}; and 23^{th}-29^{th} experiments on Fig. 5). Higher HTC reaction severities are beneficial to increase gas formation but circularity considerations call the attention on the neutralisation of volatiles-rich hydrothermal wastewaters. The co-produced aqueous phase could be suitably recirculated in hydrothermal liquefaction or carbonisation processes to increase the formation of bio-crude and hydrochar, and decrease the environmental and economic cost of the disposal of process wastewaters (Leng et al., 2020). Another circularity element could be the utilisation of the aquaous phase in the cultivation of microalgae. Tsarpali et al. (2021) reported that *Chlorella vulgaris* tolerated the HTC aqueous phase (AP) up to 7.5% in the cultivation broth and indicated that the AP is an effective nutrient source for algae that can potentially reduce the production cost of aquatic biomass.

3.5. The effects of combined severity factor and feedstock concentration on gas formation

The experimental results demonstrate that HTC biogas evolution can be improved by employing higher reaction temperature, performing hydrotreatment with a longer reaction time and applying formic acid-mediated feed suspension. The total gas yield is raised from 1.67 mol kg^{-1} to 13.42 mol kg^{-1} by using 10 wt.% CSR at 220 °C and 90 min residence time. The results show that the feedstock concentration is a critical parameter in gas formation. The highest hydrogen mole fractions are achieved using formic acid-assisted conversions at an FSR level of 12.5 wt.%. Decreasing the FSR and CSR to 5 wt.% reduced the total gas yield and hydrogen mole fraction to 7.70 mol kg^{-1} and 16.87 mol% (Table 1). Raising the FSR to 20 wt.% at a CSR level of 5 wt.% had a negative effect on hydrogen evolution and decreased the H_2 yield to 0.224 mol kg^{-1}. These experimental results suggest interacting effects between the levels of the combined severity factor and feedstock-to-suspension ratio process parameters.

Fig. 6a illustrates the HTC gas yield by components as a function of the CSF. The HTC biogas contains mainly carbon dioxide at low reaction severities (CSF <0). The yield of other gas components (H_2, CH_4, CO, C_2H_4, C_2H_6) remains low (<0.13 mol kg^{-1}) at negative CSF experimental conditions. Harsher severity conditions (CSF ⩾1.5) result in a

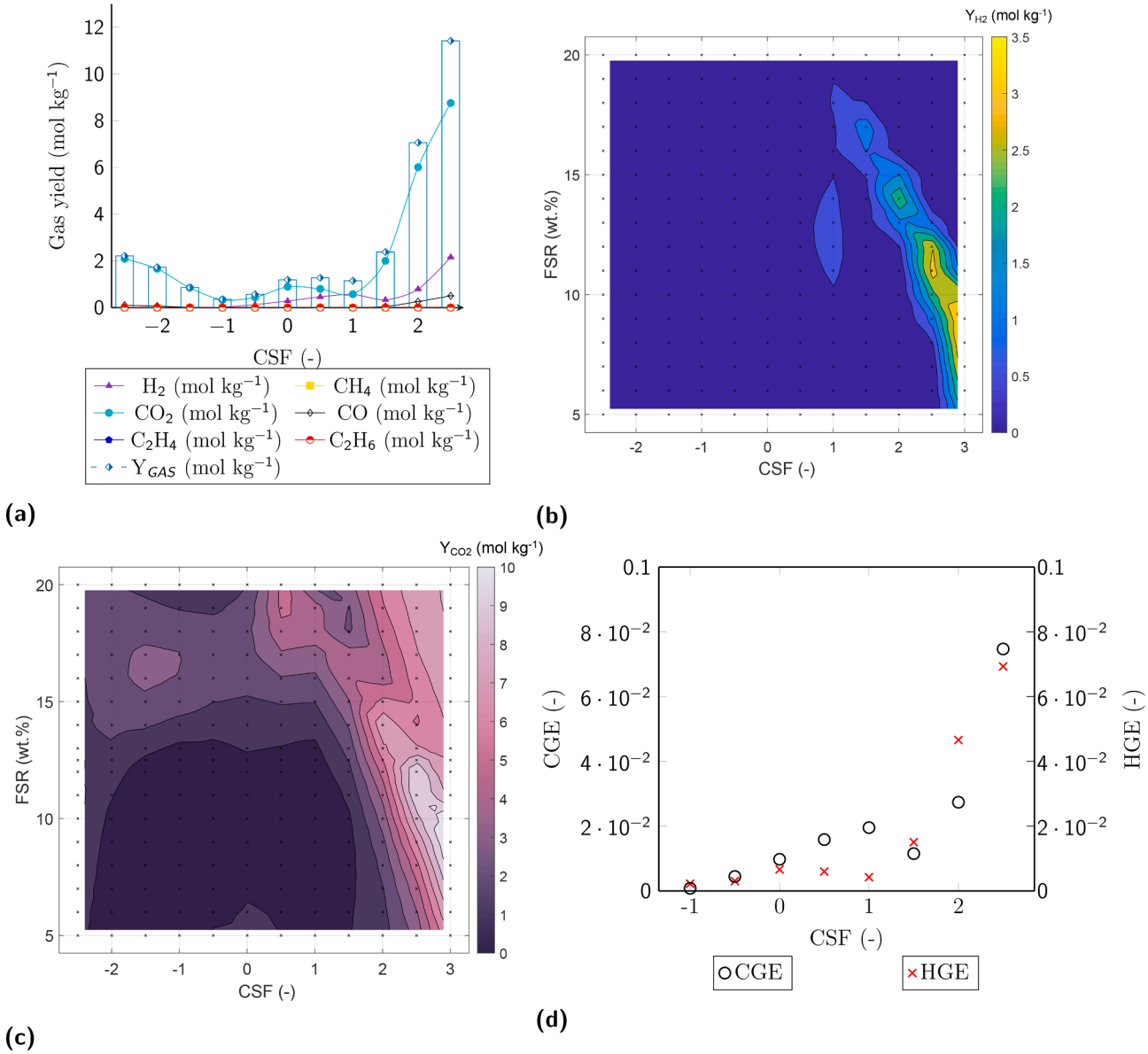

Fig. 6. The effects of HTC process parameters on (a) gas formation, (b) green hydrogen yield, (c) carbon dioxide yield, and (d) carbon- and hydrogen gasification efficiencies.

substantially increased biogas formation. Exponential growth is observed in the total gas yield between 1.0 and 2.5 combined severity factors. Fig. 6b shows that hydrogen formation outsets above 0.75 severities and the H_2 evolution intensifies above 1.50 CSF. Converting the biomass feedstock at positive CSF conditions decrease the mole fraction of CO_2 in the produced gas mixture; however, the yield of CO_2 increases significantly from 0.33 mol kg^{-1} (CSF = −1, FSR = 12.5 wt.%) to 8.76 mol kg^{-1} (CSF = 2.5, FSR = 12.5 wt.%). It is obtained that the mole fraction of CO increases within the gas mixture when the combined severity factor is raised above 0.

Figs. 6b and 6c demonstrate that the concentration of microalgae is a determinant factor in HTC gas formation. Elevated hydrogen yield (Y_{H_2} > 2.5 mol kg^{-1}) can be achieved by applying 10 wt.% ⩽ FSR ⩽12 wt.% at CSF = 2.5 reaction conditions. In the case of more dilute feedstock suspensions (FSR <10 wt.%), the combined severity factor oughts to be increased (CSF >2.8) to maintain elevated hydrogen yield (3 mol kg^{-1}). More dilute suspensions contain less transformable organic feedstock; thus, the reaction severity needs to be augmented to enhance and maintain the formation of more volatile compounds. The need for higher combined severities in the case of dilute suspensions elevates resource use (e.g., heat or the amount of formic acid) that could potentially impact the economics and environmental performance of the acid-mediated hydrothermal conversion. For this reason, the scale-up of acid-mediated HTC is subjected to taking into consideration the strong interaction between CSF and FSR factors to determine optimal working conditions for enhanced gas production. Farobie et al. (2021) reported H_2 yields between 1.70 mol kg^{-1} and 9.34 mol kg^{-1} by converting *Chlorella vulgaris* microalgae at 405 °C and 550 °C via hydrothermal gasification. The maximum hydrogen yield achieved by the formic acid-mediated hydrothermal carbonisation of *Chlorella vulgaris* is 3.04 mol kg^{-1} at a CSF of 2.43 and 12.5 wt.% feedstock concentration levels. This result demonstrates that the homogeneously catalysed hydrothermal carbonisation process is capable of providing similar hydrogen evolution compared to other high-temperature thermochemical conversion methods with potential energy-saving benefits due to the applied lower HTC temperature regimes (T_r < 250 °C).

The carbon and hydrogen gasification efficiencies are illustrated in Fig. 6d. The results show that elevated CSF levels positively affect both indicators. The CGI is increased by one order of magnitude from 0.0020 to 0.0693 when the CSF is raised from −1 to 2.5. The hydrogen formation is more significant within the mentioned CSF interval, and the value of HGE is augmented from 0.0008 to 0.0747. Gasification efficiencies are improved significantly above CSF = 1.5. Combining high combined severity factors (CSF >2.0) with lower feedstock concentration (FSR <15.0 wt.%) increases the CO_2 yield (Fig. 6c). It is obtained that the CO_2 yield of the HTC process ranges from 0.36 mol kg^{-1} to 9.63 mol kg^{-1}. Despite the relatively high CO_2 yields at elevated severity conditions (CSF >2.0), the carbon gasification efficiency remains below 0.10. This value indicates that at higher HTC severities (2.0 < CSF <3.0), hydrochar formation is combined with elevated gaseous co-product evolution. Chen et al. (2022) applied a batch reactor to gasify sewage sludge at 550–750 °C and obtained CO_2 yields between 6.50 mol kg^{-1} and 12.90 mol kg^{-1}. Raheem et al. (2021) obtained CO_2 yields between 2.5 mol kg^{-1} and 3.5 mol kg^{-1} by converting *Chlorella vulgaris* via catalytic and non-catalytic gasification. These values indicate that the CO_2 yield of formic acid-assisted hydrothermal carbonisation is in the similar range as reported in the case of other thermochemical technologies and feedstock types, making the HTC process an attractive alternative for the conversion of dilute aquatic biomass as is microalgae. The co-production of H_2 and CO_2 is beneficial considering subsequent valorisation routes, such as Power-to-X applications. The hydrothermal carbonisation process is typically carried out at moderate temperature levels (i.e. <250 °C) compared to other thermochemical processes (e.g., pyrolysis (350–550 °C), atmospheric gasification (700–900 °C), supercritical water gasification (450–800 °C)). Applying low-temperature levels during the conversion of biogenic feedstocks can be translated into lower energy demands and opens possibilities for various waste heat integration scenarios. A technical report prepared by ECRA (2016) indicated that the hydrothermal carbonisation process could offer substantial energy savings for treating high-moisture-containing biogenic wastes in cement plants. The acid-assisted hydrothermal carbonisation could be suitably integrated into already installed conventional production lines to lower environmental impacts via waste heat utilisation and thermal energy substitution with alternative fuels (Nhuchhen et al., 2021), such as stable hydrochars with a long shelf life. The elevated total gas yield and H_2 mole fraction during the hydrothermal carbonisation of *Chlorella vulgaris* offer an alternative solution to co-produce a green H_2-rich synthesis gas mixture and hydrochar, providing an additional layer to tackle the transition towards net zero emissions.

4. Conclusions

In this study, an alternative biomass-to-green hydrogen synthesis scenario is examined using acid-mediated hydrothermal carbonisation (HTC). The hydrogen and total HTC gas production is enhanced significantly and modelled along with the formation and characteristics of hydrochar and HTC liquid using the toolsets of machine learning. Harsher combined severity conditions (CSR >1.5) increase the evolution of H_2, CO_2 and CO. It is determined that there is an interaction between the combined severity factor and feedstock-to-suspension ratio parameters that influences the formation of HTC products. The production of H_2 at moderate reaction conditions offers energy-saving benefits over high-temperature thermochemical conversion methods.

CRediT authorship contribution statement

Zita Gruber: Investigation, Conceptualization, Formal analysis, Visualization. **Andras Jozsef Toth:** Funding acquisition. **Alfréd Menyhárd:** Resources, Methodology. **Peter Mizsey:** Funding acquisition. **Mikołaj Owsianiak:** Writing - review & editing. **Daniel Fozer:** Writing - review & editing, Conceptualization, Investigation, Formal analysis, Visualization, Supervision.

Declaration of Competing Interest

The authors declare that they have no known competing financial interests or personal relationships that could have appeared to influence the work reported in this paper.

Acknowledgement

The authors are grateful for the financial support from the Hungarian National Scientific Research Foundation (OTKA) projects: nr.: 128543 and nr.: 131586. The research was supported by the EU LIFE program, LIFE-CLIMCOOP project (LIFE19 CCA/HU/001320).

Appendix A. Supplementary data

Supplementary data associated with this article can be found, in the online version, athttps://doi.org/10.1016/j.biortech.2022.128071.

References

Adedeji, O.M., Russack, J.S., Molnar, L.A., Bauer, S.K., 2022. Co-Hydrothermal Liquefaction of Sewage Sludge and Beverage Waste for High-Quality Bio-energy Production. Fuel 324, 124757. https://doi.org/10.1016/j.fuel.2022.124757.

Behera, B., Mari Selvam, S., Balasubramanian, P., 2022. Hydrothermal processing of microalgal biomass: Circular bio-economy perspectives for addressing food-water-energy nexus. Bioresour. Technol. 359, 127443 https://doi.org/10.1016/j.biortech.2022.127443.

Bi, H., Wang, C., Jiang, X., Jiang, C., Bao, L., Lin, Q., 2021. Thermodynamics, kinetics, gas emissions and artificial neural network modeling of co-pyrolysis of sewage sludge and peanut shell. Fuel 284, 118988. https://doi.org/10.1016/j.fuel.2020.118988.

Burden, F., Winkler, D., 2009. Bayesian Regularization of Neural Networks. Humana Press, Totowa, NJ 23–42. https://doi.org/10.1007/978-1-60327-101-1_3.
Calijuri, M.L., Silva, T.A., Magalhães, I.B., de Paula Pereira, A.S.A., Marangon, B.B., de Assis, L.R., Lorentz, J.F., 2022. Bioproducts from microalgae biomass: Technology, sustainability, challenges and opportunities. Chemosphere 305, 135508. https://doi.org/10.1016/j.chemosphere.2022.135508.
Chen, H., Fu, Q., Liao, Q., Zhu, X., Shah, A., 2021. Applying artificial neural network to predict the viscosity of microalgae slurry in hydrothermal hydrolysis process. Energy AI 4, 100053. https://doi.org/10.1016/j.egyai.2021.100053.
Chen, S., Mowery, R., Chambliss, C., van Walsum, G., 2007. Pseudo reaction kinetics of organic degradation products in dilute-acid-catalyzed corn stover pretreatment hydrolysates. Biotechnol Bioeng 98, 1135–1145. https://doi.org/10.1002/bit.21480.
Chen, Y., Yi, L., Wei, W., Jin, H., Guo, L., 2022. Hydrogen production by sewage sludge gasification in supercritical water with high heating rate batch reactor. Energy 238, 121740. https://doi.org/10.1016/j.energy.2021.121740.
Chum, H.L., Johnson, D.K., Black, S.K., Overend, R.P., 1990. Pretreatment-Catalyst effects and the combined severity parameter. Appl. Biochem. Biotechnol. 24, 1–14. https://doi.org/10.1007/BF02920229.
Dashti, A., Noushabadi, A.S., Raji, M., Razmi, A., Ceylan, S., Mohammadi, A.H., 2019. Estimation of biomass higher heating value (HHV) based on the proximate analysis: Smart modeling and correlation. Fuel 257, 115931. https://doi.org/10.1016/j.fuel.2019.115931.
ECRA, 2016. European Cement Research Academy: Evaluation of the energy performance of cement kilns in the context of co-processing. Technical Report. URL: https://cembureau.eu/media/oyahklgk/12042-ecra-energy-performance-cement-kilns-2017-10-15.pdf. accessed 28.08.2022.
Evcil, T., Simsir, H., Ucar, S., Tekin, K., Karagoz, S., 2020. Hydrothermal carbonization of lignocellulosic biomass and effects of combined Lewis and Brønsted acid catalysts. Fuel 279, 118458. https://doi.org/10.1016/j.fuel.2020.118458.
Farobie, O., Matsumura, Y., Syaftika, N., Amrullah, A., Hartulistiyoso, E., Bayu, A., Moheimani, N.R., Karnjanakom, S., Saefurahman, G., 2021. Recent advancement on hydrogen production from macroalgae via supercritical water gasification. Bioresour. Technol. Rep. 16, 100844 https://doi.org/10.1016/j.biteb.2021.100844.
Fózer, D., Tóth, A.J., Varbanov, P.S., Klemeš, J.J., Mizsey, P., 2021. Sustainability assessment of biomethanol production via hydrothermal gasification supported by artificial neural network. J. Cleaner Prod. 318, 128606 https://doi.org/10.1016/j.jclepro.2021.128606.
Henry, A., Prasher, R., Majumdar, A., 2020. Five thermal energy grand challenges for decarbonization. Nature Energy 5, 635–637. https://doi.org/10.1038/s41560-020-0675-9.
Huang, Y., Chen, M., Li, Q., Xing, W., 2018. Hydrogen-rich syngas produced from co-gasification of wet sewage sludge and torrefied biomass in self-generated steam agent. Energy 161, 202–213. https://doi.org/10.1016/j.energy.2018.07.097.
IEA, 2021. Hydrogen. Technical Report. International Energy Agency. URL: https://www.iea.org/reports/hydrogen. accessed 28.08.2022.
Iñiguez, M.E., Conesa, J.A., Fullana, A., 2019. Hydrothermal carbonization (HTC) of marine plastic debris. Fuel 257, 116033. https://doi.org/10.1016/j.fuel.2019.116033.
Islam, M.B., Khalekuzzaman, M., Kabir, S.B., Hossain, M.R., 2022. Shrimp waste-derived chitosan harvested microalgae for the production of high-quality biocrude through hydrothermal liquefaction. Fuel 320, 123906. https://doi.org/10.1016/j.fuel.2022.123906.
Khoo, C.G., Lam, M.K., Mohamed, A.R., Lee, K.T., 2020. Hydrochar production from high-ash low-lipid microalgal biomass via hydrothermal carbonization: Effects of operational parameters and products characterization. Environ. Res. 188, 109828 https://doi.org/10.1016/j.envres.2020.109828.
Lachos-Perez, D., César Torres-Mayanga, P., Abaide, E.R., Zabot, G.L., De Castilhos, F., 2022. Hydrothermal carbonization and Liquefaction: differences, progress, challenges, and opportunities. Bioresour. Technol. 343, 126084 https://doi.org/10.1016/j.biortech.2021.126084.
Leng, L., Huang, H., Li, H., Li, J., Zhou, W., 2019. Biochar stability assessment methods: A review. Sci. Total Environ. 647, 210–222. https://doi.org/10.1016/j.scitotenv.2018.07.402.
Leng, S., Leng, L., Chen, L., Chen, J., Chen, J., Zhou, W., 2020. The effect of aqueous phase recirculation on hydrothermal liquefaction/carbonization of biomass: A review. Bioresour. Technol. 318, 124081 https://doi.org/10.1016/j.biortech.2020.124081.
Liu, L., Zhai, Y., Liu, X., Liu, X., Wang, Z., Zhu, Y., Xu, M., 2022. Features and mechanisms of sewage sludge hydrothermal carbonization aqueous phase after ferrous/persulfate-based process: The selective effect of oxidation and coagulation. J. Clean. Prod. 366, 132831 https://doi.org/10.1016/j.jclepro.2022.132831.
Liu, X., Fan, Y., Zhai, Y., Liu, X., Wang, Z., Zhu, Y., Shi, H., Li, C., Zhu, Y., 2022. Co-hydrothermal carbonization of rape straw and microalgae: pH-enhanced carbonization process to obtain clean hydrochar. Energy 257, 124733. https://doi.org/10.1016/j.energy.2022.124733.
Lu, J., Wang, S., Li, Q., Xu, S., Wang, C., Wu, Y., 2022. Catalytic hydrothermal liquefaction of microalgae to bio-oil with in-situ hydrogen donor formic acid. J. Anal. Appl. Pyrol. 105653 https://doi.org/10.1016/j.jaap.2022.105653.
MathWorks, 2021. Matlab R2021a. URL: https://se.mathworks.com/products/new_products/release2021a.html. accessed: 28.08.2022.
Min, K.H., Kim, D.H., Ki, M.R., Pack, S.P., 2022. Recent progress in flocculation, dewatering, and drying technologies for microalgae utilization: Scalable and low-cost harvesting process development. Bioresour. Technol. 344, 126404 https://doi.org/10.1016/j.biortech.2021.126404.
Morales-Contreras, B.E., Flórez-Fernández, N., Dolores Torres, M., Domínguez, H., Rodríguez-Jasso, R.M., Ruiz, H.A., 2022. Hydrothermal systems to obtain high value-added compounds from macroalgae for bioeconomy and biorefineries. Bioresour. Technol. 343, 126017 https://doi.org/10.1016/j.biortech.2021.126017.
Nhuchhen, D.R., Sit, S.P., Layzell, D.B., 2021. Alternative fuels co-fired with natural gas in the pre-calciner of a cement plant: Energy and material flows. Fuel 295, 120544. https://doi.org/10.1016/j.fuel.2021.120544.
Owsianiak, M., Brooks, J., Renz, M., Laurent, A., 2018. Evaluating climate change mitigation potential of hydrochars: compounding insights from three different indicators. GCB Bioenergy 10, 230–245. https://doi.org/10.1111/gcbb.12484.
Parikh, J., Channiwala, S., Ghosal, G., 2007. A correlation for calculating elemental composition from proximate analysis of biomass materials. Fuel 86, 1710–1719. https://doi.org/10.1016/j.fuel.2006.12.029.
Raheem, A., Abbasi, S.A., Mangi, F.H., Ahmed, S., He, Q., Ding, L., Memon, A.A., Zhao, M., Yu, G., 2021. Gasification of algal residue for synthesis gas production. Algal Res. 58, 102411 https://doi.org/10.1016/j.algal.2021.102411.
Rajagopal, J., Gopinath, K.P., Neha, R., Aakriti, K., Jayaraman, R.S., Arun, J., Pugazhendhi, A., 2022. Processing of household waste via hydrothermal gasification and hydrothermal liquefaction for bio-oil and bio-hydrogen production: Comparison with RSM studies. J. Environ. Chem. Eng. 10, 107218 https://doi.org/10.1016/j.jece.2022.107218.
Sarrion, A., de la Rubia, A., Coronella, C., Mohedano, A.F., Diaz, E., 2022. Acid-mediated hydrothermal treatment of sewage sludge for nutrient recovery. Sci. Total Environ. 838, 156494 https://doi.org/10.1016/j.scitotenv.2022.156494.
de Siqueira Castro, J., Assemany, P.P., de Oliveira Carneiro, A.C., Ferreira, J., de Jesus Júnior, M.M., de Ávila Rodrigues, F., Calijuri, M.L., 2021. Hydrothermal carbonization of microalgae biomass produced in agro-industrial effluent: Products, characterization and applications. Sci. Total Environ. 768, 144480 https://doi.org/10.1016/j.scitotenv.2020.144480.
Soria-Verdugo, A., Goos, E., García-Hernando, N., Riedel, U., 2018. Analyzing the pyrolysis kinetics of several microalgae species by various differential and integral isoconversional kinetic methods and the Distributed Activation Energy Model. Algal Res. 32, 11–29. https://doi.org/10.1016/j.algal.2018.03.005.
Tiong, L., Komiyama, M., 2022. Statistical analysis of microalgae supercritical water gasification: Reaction variables, catalysis and reaction pathways. J. Supercritical Fluids 183, 105552. https://doi.org/10.1016/j.supflu.2022.105552.
Tsarpali, M., Arora, N., Kuhn, J.N., Philippidis, G.P., 2021. Beneficial use of the aqueous phase generated during hydrothermal carbonization of algae as nutrient source for algae cultivation. Algal Res. 60, 102485 https://doi.org/10.1016/j.algal.2021.102485.
Vyazovkin, S., Burnham, A.K., Criado, J.M., Pérez-Maqueda, L.A., Popescu, C., Sbirrazzuoli, N., 2011. ICTAC Kinetics Committee recommendations for performing kinetic computations on thermal analysis data. Thermochim. Acta 520, 1–19. https://doi.org/10.1016/j.tca.2011.03.034.
Wang, T., Zhai, Y., Zhu, Y., Li, C., Zeng, G., 2018. A review of the hydrothermal carbonization of biomass waste for hydrochar formation: Process conditions, fundamentals, and physicochemical properties. Renew. Sustain. Energy Rev. 90, 223–247. https://doi.org/10.1016/j.rser.2018.03.071.
Xie, L.F., Duan, P.G., Jiao, J.L., Xu, Y.P., 2019. Hydrothermal gasification of microalgae over nickel catalysts for production of hydrogen-rich fuel gas: Effect of zeolite supports. Int. J. Hydrogen Energy 44, 5114–5124. doi: 10.1016/j.ijhydene.2018.09.175. the 6th International Conference on Energy, Engineerisng and Environmental Engineering.
Xu, Z., Qi, R., Xiong, M., Zhang, D., Gu, H., Chen, W., 2021. Conversion of cotton textile waste to clean solid fuel via surfactant-assisted hydrothermal carbonization: Mechanisms and combustion behaviors. Bioresour. Technol. 321, 124450 https://doi.org/10.1016/j.biortech.2020.124450.
Yang, G., Liu, H., Li, Y., Zhou, Q., Jin, M., Xiao, H., Yao, H., 2022. Kinetics of hydrothermal carbonization of kitchen waste based on multi-component reaction mechanism. Fuel 324, 124693. https://doi.org/10.1016/j.fuel.2022.124693.
Ye, B., Zhang, R., Cao, J., Lei, K., Liu, D., 2020. The study of co-combustion characteristics of coal and microalgae by single particle combustion and TGA methods. J. Energy Inst. 93, 508–517. https://doi.org/10.1016/j.joei.2019.07.001.
Zhang, S., Sheng, K., Yan, W., Liu, J., Shuang, E., Yang, M., Zhang, X., 2021. Bamboo derived hydrochar microspheres fabricated by acid-assisted hydrothermal carbonization. Chemosphere 263, 128093. https://doi.org/10.1016/j.chemosphere.2020.128093.
Zhang, Z., Yang, J., Qian, J., Zhao, Y., Wang, T., Zhai, Y., 2021. Biowaste hydrothermal carbonization for hydrochar valorization: Skeleton structure, conversion pathways and clean biofuel applications. Bioresour. Technol. 324, 124686 https://doi.org/10.1016/j.biortech.2021.124686.
Zhu, X., Li, Y., Wang, X., 2019. Machine learning prediction of biochar yield and carbon contents in biochar based on biomass characteristics and pyrolysis conditions. Bioresour. Technol. 288, 121527 https://doi.org/10.1016/j.biortech.2019.121527.